Near Surface Geophysics

EAGE EUROPEAN ASSOCIATION OF GEOSCIENTISTS & ENGINEERS

Near Surface Geophysics, 2018, **16**, 593–610 doi: 10.1002/nsg.12011

High-resolution reflection seismics reveal the structure and the evolution of the Quaternary glacial Tannwald Basin

Thomas Burschil[1]*, Hermann Buness[1], David C. Tanner[1], Ulrike Wielandt-Schuster[2], Dietrich Ellwanger[2] and Gerald Gabriel[1]

[1]*Leibniz Institute for Applied Geophysics (LIAG), Stilleweg 2, Hannover D-30655, Germany, and* [2]*Regierungspräsidium Freiburg, Landesamt für Geologie, Rohstoffe und Bergbau (LGRB), Albertstraße 5, Freiburg im Breisgau D-79104, Germany*

Received December 2017, revision accepted June 2018

ABSTRACT

Over-deepened basins exist throughout the Alpine realm. Improving our knowledge on these basins is of high social relevance, since these areas are often well-populated and they possess, for instance, unusual hydrological settings. Nonetheless, geophysical and sedimentological investigations of over-deepened basins are rare. We analyse the sedimentary succession of such a basin, the Tannwald Basin, through geological interpretation of seismic reflection profiles. The basin is located approximately 60 km north of the European Alps. It was incised into Tertiary molasse sediments by the Rhine Glacier and later filled by glacial, fluvial, and lacustrine deposits of 250 m thickness. The Leibniz Institute for Applied Geophysics acquired a grid of five high-resolution seismic reflection lines that imaged till the deepest parts of the Tannwald Basin. The seismic profiles, processed to a pre-stack depth migration level, allow a detailed geological interpretation that is calibrated with the help of a nearby borehole. We determine the structure and the seismic facies of the sediment succession in the basin and presume the following hypothesis of the evolution of the basin: sub-glacial erosion comprises the excavation of the over-deepened basin as well as detachment of large fragments of molasse material. These molasse slabs were deposited within the basin in a layer of basal till that graded upwards in water-lain till and fine-grained deposits. During the last two glaciations, the basinal structure became buried by till sequences and glacio-fluvial sediments.

Key words: high-resolution seismic, seismic interpretation, seismic lithology.

INTRODUCTION

The European Alps are surrounded by an apron of glacially eroded, over-deepened valleys and basins, filled with glacial, fluvial and/or lacustrine sediments. The term 'over-deepened' relates to the genesis of these valleys and basins, which are of glacial origin. It is assumed that they were formed by pressurized sub-glacial melt water below the glaciers (Huuse and Lykke-Andersen 2000). Understanding the geological evolution of the over-deepened Alpine valleys is of high scientific and societal importance (MacGregor *et al.* 2000; Anderson, Molnar and Kessler 2006; Preusser, Reitner and Schlüchter 2010). New approaches to access, compare and correlate the information that is archived in the sediments of these valleys will be undertaken in the International Continental Scientific Drilling Program (ICDP) project 'Drilling Over-deepened Alpine Valleys' (DOVE; Anselmetti *et al.* 2016). Scientific drillings, distributed throughout the entire Alpine

*E-mail: Thomas.Burschil@leibniz-liag.de

realm, should allow a reconstruction of its climatically driven glaciation history.

Repeated glacial advances and retreats during the Quaternary resulted in a complex distribution of over-deepened basins that were refilled by glacial and post-glacial deposits (Ellwanger *et al.* 2011). Consequently, boreholes that directly access the sediments have only limited access to the three-dimensional distribution of different sediment sequences in the basins (van Husen and Mayer, 2007). In contrast, geophysical surveys are capable of determining the shape and characterizing the infill of the basins. Among the geophysical methods, the seismic reflection method yields the highest resolution to image the whole infill (e.g. Pfiffner *et al.* 1997; Nitsche *et al.* 2002; Brückl *et al.* 2010; Reitner *et al.* 2010). High-resolution seismic data are usually acquired on lakes (van Rensbergen *et al.* 1998, 1999; Morend, Pugin and Gorin 2002); onshore seismic data with a sufficient amount of detail are rare (e.g. Büker, Green and Horstmeyer 1998, 2000).

In contrast to studies of proximal basins (Pfiffner *et al.* 1997; van Rensbergen *et al.* 1998, 1999; de Franco *et al.* 2009; Barnaba *et al.* 2010; Brückl *et al.* 2010; Reitner *et al.* 2010; Dehnert *et al.* 2012; Buechi *et al.* 2017; Pomper *et al.* 2017), only a few geophysical data are available from over-deepened basins in the German part of the Alpine foreland (Ehlers and Gibbard 2004; Ellwanger *et al.* 2011). These basins are typically located distally to the corresponding catchment areas. Hence, the sedimentary processes that occur as a response to the advances and retreats of the glaciers probably differ from those within the intra-mountain basins.

One such distal basin is the Tannwald Basin in southwest Germany, a branch basin of a pre-Holsteinian advance of the Rhine Glacier. It has been chosen as one of the drill sites of DOVE. First evidence for an over-deepening in this area was the sedimentary succession found in the Schneidermartin research borehole, drilled in 1993/1994. It was confirmed by a refraction seismic survey of Behnke and Bram (1998), but without further details on the extent, shape, or orientation of the structure.

In this paper, we investigate the Tannwald Basin using high-resolution seismic reflection methods with the aim to characterize this over-deepened basin. We image the shape of the basin and the sedimentary facies that occur in the basin fill. The seismic interpretations are calibrated using the sediment succession of the Schneidermartin research borehole. Using these data, we postulate the probable geological evolution of the basin.

GEOLOGICAL SETTING

The Alpine Orogeny began during the Miocene, as the African plate was thrust over the European plate (Pfiffner 2014). This caused the formation of the wedge-shaped North Alpine molasse foreland basin (Pfiffner 1986), which is still undergoing Alpine deformation (Pfiffner 1986; Ziegler, Cloetingh and van Wees 1995; von Hartmann, Tanner and Schumacher 2016).

The orogenic development had a major influence on the river network and therefore on the erosion and sedimentation processes. Between 11 and 6 Myr B.P., an early Danube river system developed northwards of the Alps, in the area presently occupied by the rivers Rhone and Aare. It flowed from west to east towards the Pannonian Basin. During the Late Pliocene, this system was interrupted when its western part was captured by the river Rhine (e.g. Boenigk 1987). Hence, this part achieved its present-day drainage towards the North Sea and the remaining Danube river system began only eastwards of the Upper Rhine Graben.

In the Early Pleistocene, the Alpine Rhine took its present-day course, thus changing this part of the landscape of the Alps (Ellwanger, Lämmermann-Barthel and Neeb 2003; Pfiffner 2014). In this sector of the Alpine foreland, three terrace gravel units (named Donau, Gunz, and Mindel) show the increase in size of the Rhenish Alpine catchment area over time.

Climate-controlled landscape evolution by glacial over-deepening took place only in the Middle-Late Pleistocene (Preusser *et al.* 2010; Ellwanger *et al.* 2011). In the Rhine Glacier area, Ellwanger *et al.* (2011) differentiated three main formations based on lithostratigraphy (Fig. 1). They are, from oldest to youngest, the Dietmanns Fm., Illmensee Fm., and Hasenweiler Fm. (Table 1; cf. Litholex 2017). In terms of chronostratigraphy, each of them comprises parts of two adjacent glacial stages, that is, Hosskirchian–Rissian, Rissian–Wurmian, and the Wurmian–present, respectively (Table 1). Each formation shows good evidence of two separate ice advances of the Rhine Glacier. The formations are bound by unconformities, which are termed, from oldest to youngest, D3 to D1 (Table 1; Ellwanger *et al.* 2011).

The study area is the Tannwald Basin, located at the terminal moraine of the last glacial maximum (LGM) (Fig. 1). In the study area, the occurrence of a thick sequence of Quaternary glacial sediments overlying molasse sediments was drilled in the Schneidermartin research borehole in 1993/1994 (Fig. 2). In the borehole, a succession of glacial and meltwater deposits of the Dietmanns Fm. and the Illmensee Fm. was unveiled. At the base of the basin, there is nearly 15 m of molasse material that is distinct from the underlying

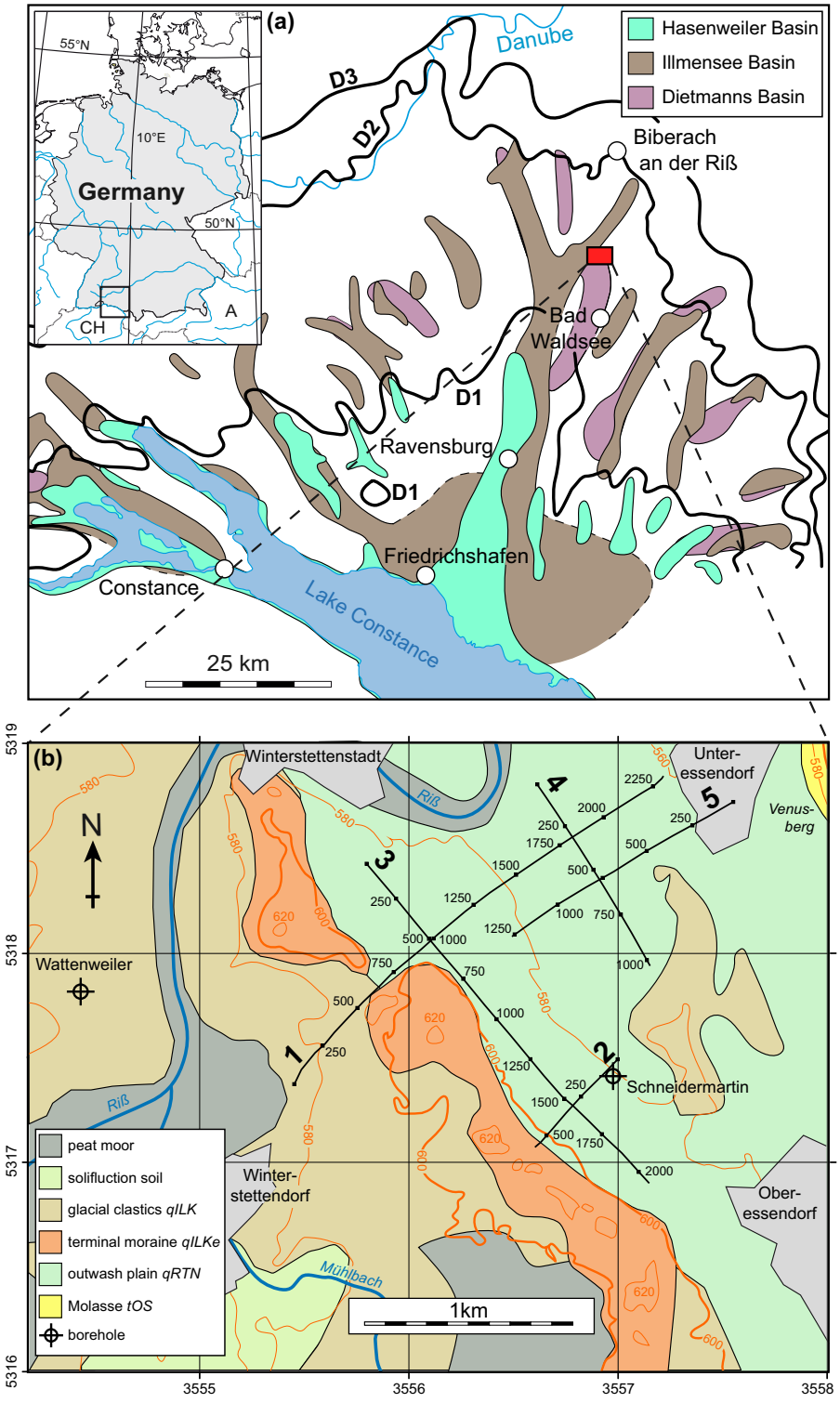

Figure 1 (a) Map of basins of the Rhine Glacier, modified after Ellwanger *et al.* (2011). The basins are generally younger and deeper towards a more proximal position with respect to the glacier. Three different generations of basins can be identified, bounded by D1–D3 unconformities (see Table 1). The maximum geographical extent of the unconformities is indicated; they correspond to the advances of the glaciers in the Wurmian, Rissian and Hosskirchian ice ages. (b) Geological map of the survey area of the Tannwald Basin showing the location of reflection profiles 1–5 and two borehole locations used in the interpretation.

Table 1 Chrono- and Lithostratigraphic System of Rhine Glacier Sediments, modified after Ellwanger *et al.* (2011)

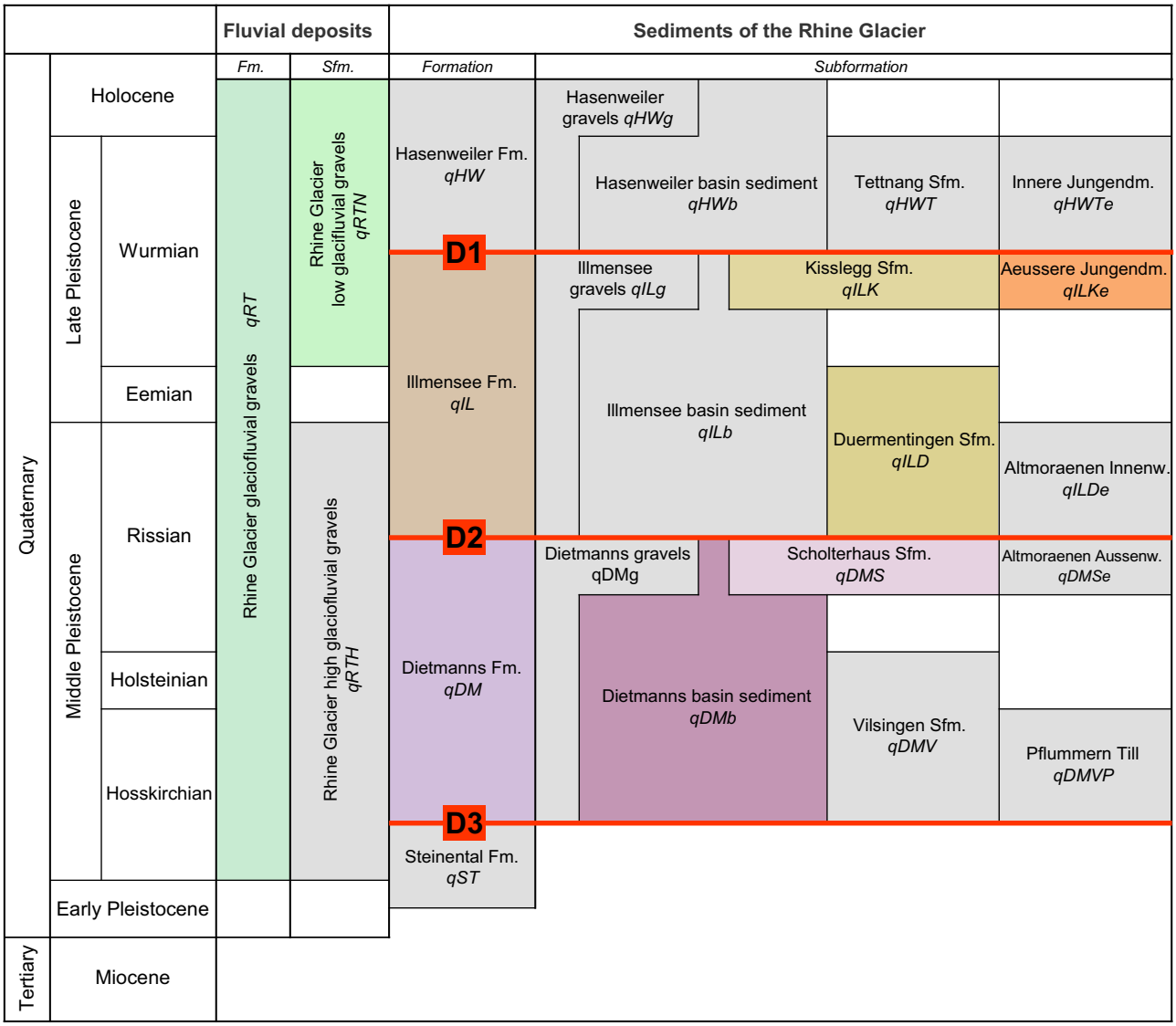

molasse substrate (Fig. 2). It contains numerous shear horizons and is therefore considered allochthonous (LGRB 2015). The infill of glacial and melt-water deposits began with a 150-m thick sequence of aggrading water-lain till and laminated fines, which is overlain by a prograding system composed of sands and silts. The basin infill is conformably overlain by a succession of glacial and melt-water deposits pertaining to three younger ice advances (cf. Table 1): a 17-m thick package of the Scholterhaus advance (Dietmanns Fm., Rissian stage), a 7-m thick package of the Duermentingen advance (Illmensee Fm., Rissian stage) and finally, a 22-m thick package of the Kisslegg advance (Illmensee Fm., Wurmian stage). Another borehole, located east of Wattenweiler (Fig. 1), explored the western part of the Tannwald Basin. Unfortunately, the Wattenweiler borehole shows less resolution than the Schneidermartin borehole, with respect to the sedimentary information. It identified the erosional base of the over-deepened basin at 80-m depth. Several seismic refraction profiles were carried out by Behnke and Bram (1998) across the Tannwald Basin. They determined that its depth varied from 80 to 200 m, but they show only a few details of the basin infill.

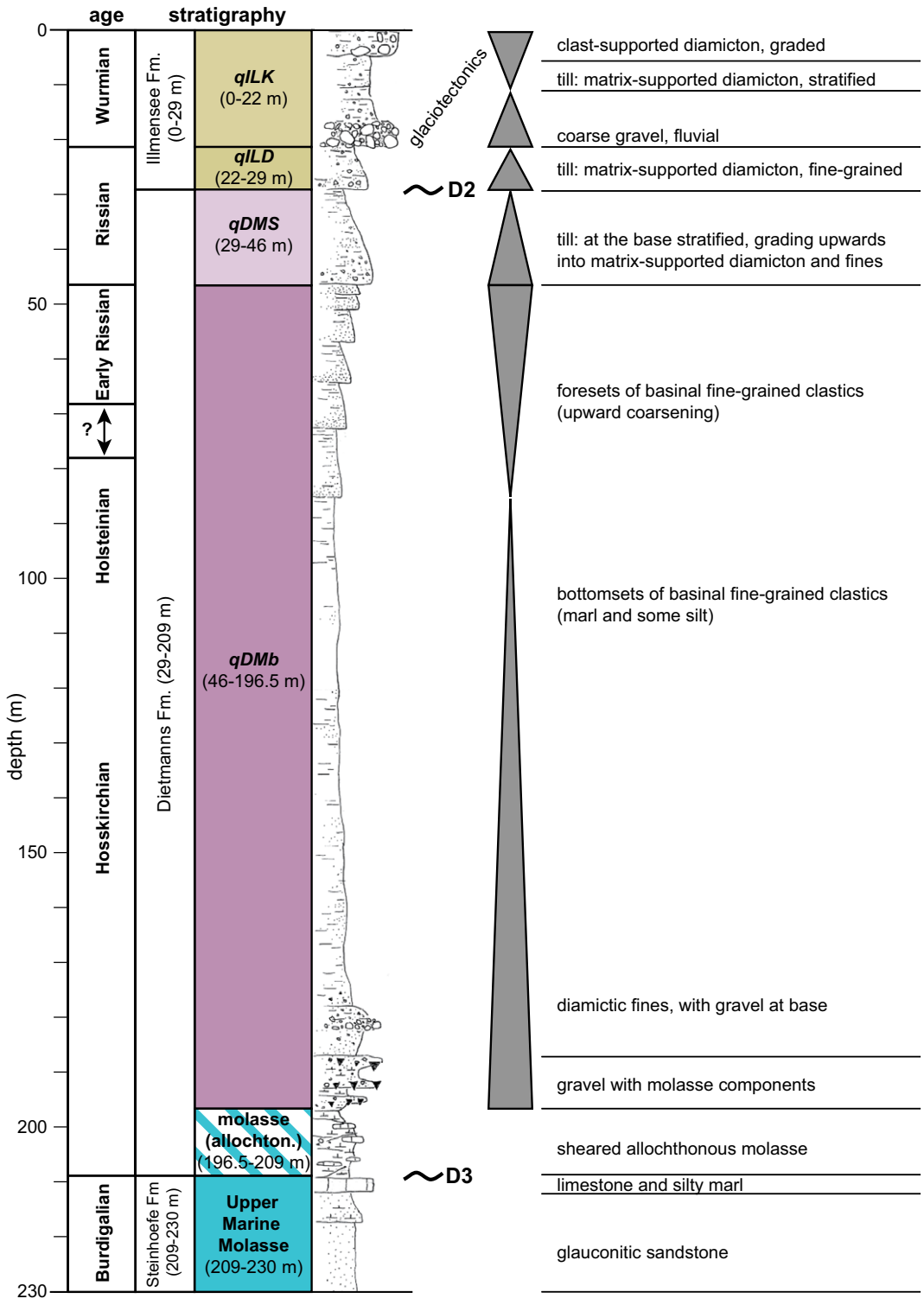

Figure 2 Interpretation of the sediment succession of the Schneidermartin research borehole. For stratigraphic names see Table 1. Fourth column shows a graphical lithology of the sediments, grey triangles denote fining-up and coarsening-up sequences (after Neeb, pers. comm. 2013; Ellewanger *et al.* 2011).

Table 2 Acquisition Parameters

Source	Hydraulic Minivibrator HVP-30
Source point spacing	5 m (*P5*: 10 m)
Vertical stack	2
Source signal	Linear sweep, 20–200 Hz, 10 s
Receiver type	Sensor SM6 geophones, vertical, 20 Hz
Receiver spacing	2.5 m (*P5*: 5 m)
No. of channels	Up to 360
Spread type	Split spread/roll along
Recording unit	Geometrics Geode
Sampling rate	1 ms
Record length	2 s
Vibroseis field correlation	on
Total number of shot points	1516

SEISMIC ACQUISITION

In 2014 and 2015, LIAG recorded five P-wave seismic reflection profiles across the north-eastern part of the Tannwald Basin (Fig. 1b). The profiles are concentrated on the deepest part of the Tannwald Basin, as known from seismic refraction surveys (Behnke and Bram 1998). The seismic grid is connected to the Schneidermartin borehole. Proceeding eastwards, the molasse outcrop at the Venusberg (see Fig. 1b) could only be approached up to 500 m due to habitation and the presence of a major road.

A dense receiver and shot spacing of 2.5 and 5.0 m, respectively, was chosen, in order to reconstruct the basin morphology and the sedimentary infill in detail. Only profile 5 was recorded using spacings of 5 and 10 m, respectively, for logistical reasons. The seismic source is represented by a small (4 t) hydraulic vibrator, developed at LIAG, that is able to excite frequencies up to 500 Hz. Based on calibration tests, we set the sweep frequencies to 20–200 Hz in this survey. The acquisition parameters are summarized in Table 2.

The data quality was generally good, reflections from inside and from the base of the basin can be easily recognized, even in the raw shot gathers (Fig. 3a). However, at some locations a significant loss in signal strength of refractions and reflections is observed (white hexagon, Fig. 3a).

SEISMIC PROCESSING

Firstly, we performed a conventional dip move-out (DMO) processing approach. After geometry assignment, the basic steps in the pre-stack processing were: static corrections, bottom mute, spectral balancing, and automatic gain control (Table 3). This pre-stack processing flow generated the best

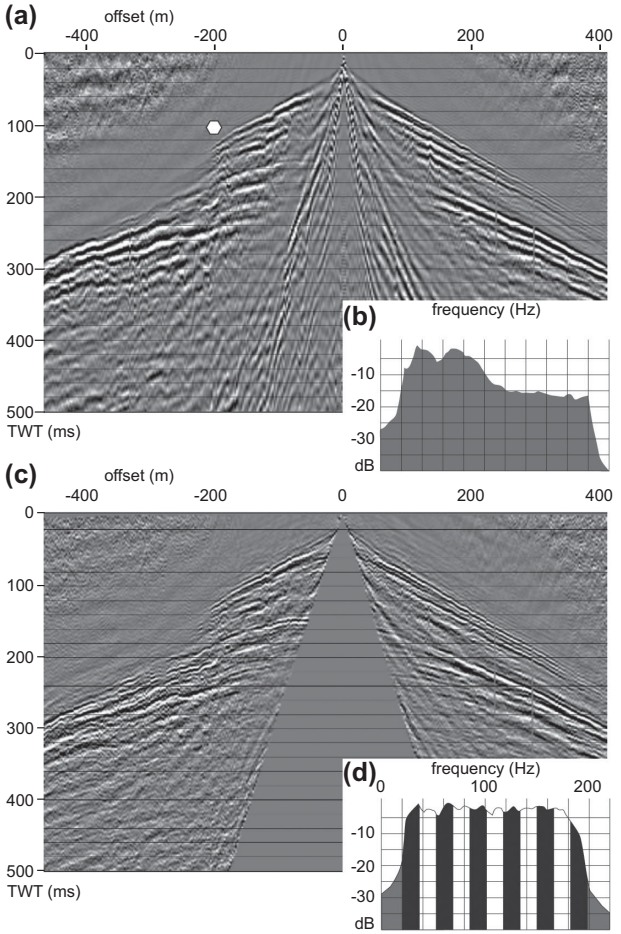

Figure 3 (a) Raw shot gather, with only automatic gain control applied, (b) with frequency spectrum for entire shot gather and (c) shot gather after pre-processing, with (d) corresponding frequency spectrum. Location of the shot is approximately 670 m on profile 1. Note the disappearance of both refractions and shallow reflections (white hexagon), corresponding to the non-reflective region at 470 m on profile 1 (Fig. 4a). The frequency spectrum (d) shows the 11 panels (black and white boxes) used for spectral balancing.

stacking results in terms of frequency content and reflection coherency (Fig. 3d). We determined seismic velocity fields from interactive velocity analysis (IVA) and performed normal move-out correction, DMO correction in common offset gathers and common midpoint stacking, and tested different post-stack migrations.

Since the results of the DMO processing approach were unsatisfactory with respect to the complex inner geological structures, we decided to use Kirchhoff pre-stack depth migration (PSDM), which produced higher quality images of reflectors, in particular in the shallow parts of the seismic profiles. Our processing flow chart is similar to that of

Table 3 Processing Parameters

Processing Step	Application
Data import	SEG2-data load to SeisSpace®
QC	Killing of bad traces
Vertical stacking	Two-fold
Geometry load	1.25 m (*5P*: 2.5 m) CMP bin interval, 2.5 m (*5P*: 5 m) absolute offset bin interval
Trace muting	Bottom mute of surface waves
Elevation statics	Smoothed topography replacement velocity 1800 m/s
Refraction statics	High-frequency part of refraction statics
Spectral balancing	Spectral whitening in 11 frequency panels between 20 and 200 Hz
Scaling	Automatic gain control (window 300 ms)
Profiles 1P, 3P, 4P, 5P:	
Residual statics	Correlation auto-statics
Pre-stack Kirchhoff depth migration	From topography, final reference datum 580 m, velocity field iteration by interactive horizon RMO analysis and ray-based tomographic inversion
Spectral balancing	Spectral whitening in 11 frequency panels between 24 and 200 Hz
F-K filtering (offset gather)	±0.6 ms per trace, 36–180 Hz accepted
F-K filtering (CRP gather)	±100 to ±3500 m/s, 25–220 Hz rejected
Trace muting	Top and bottom mute in CRP gather
CRP stacking	20% alpha trimmed mean
Profile 2P:	
NMO correction	Stacking velocity field determined from IVA, 40% stretch mute
F-K DMO	Common offset bins, single velocity field
CDP stacking	20% Alpha-trimmed mean, shift to final reference datum 580 m
F-X decon	10% White noise
Spectral balancing	11 Panels 24–200 Hz
F-K filtering (zero-offset section)	±1 ms per trace, 36–180 Hz accepted
FD time migration	Emergence angle 80°, smoothed IVA stacking velocity field, scale factor 0.5
Band-pass filter	36–180 Hz
Time-to-depth conversion	Smoothed IVA stacking velocity field

Bradford *et al.* (2006), who first showed the applicability of PSDM to shallow seismic data. The accurate velocity model required by PSDM was built using a migration velocity analysis (MVA) approach, which included residual move-out (RMO) picking on common image gathers, and a ray-based tomographic inversion. The DMO velocities served as an initial starting model. Refraction statics were restricted to the high-frequency content to correct for very local variations, but allow MVA to adapt the shallow velocity field. A crucial step proved to be data enhancement after PSDM. We tested various filtering (fk with different flanking, spatial filtering), muting (different windows) and signal shaping (spectral whitening, de-convolution) in different gathers. Best results, in terms of imaging quality, were produced by a sequence of spectral balancing and fk-filtering in common offset (COF), as well as in common reflection point (CRP) gathers and a precise top and bottom muting in CRP gathers (Table 3). We undertook some 5–10 iterations for each profile to build the final velocity model, that is, the velocity variations and the imaging quality varied only marginally after each iteration.

The seismic processing was carried out using SeisSpace® software. The processing was optimized for the upper 250 m, that is, the basin infill. We did not focus on the deeper molasse layers. Care was taken when analysing the uppermost layers, because their reflections interfere with refracted signals, shear wave reflections and guided waves. They can be best discriminated by their comparably higher frequency; otherwise we had to go back to the original pre-stack data for judgement. All depths given in this paper are referenced to the seismic datum of 580 m a.s.l.

For the very short profile 2, PSDM generated strong edge migration artefacts, so we decided to use post-stack migration of the DMO stack for the interpretation of this profile. The depth of marker horizons was adjusted at the intersection with profile 3 during time-to-depth conversion.

Depending on the local seismic velocity, the minimum wavelength of the seismic signal varies from 8 m for shallow reflections to 14 m at a depth of 200 m. This corresponds to a maximum vertical resolution of 2–3.5 m. We estimate the horizontal resolution after migration to be twice the vertical resolution, that is, 4–7 m.

GEOLOGICAL INTERPRETATION

The pre-stack depth migration (PSDM) sections (Figs. 4, 5 and 6) and a three-dimensional seismic fence diagram (Fig. 7) show the exceptional quality of the seismic profiles. We interpreted the seismic section structurally by tracing major reflectors. Geological units were calibrated with the stratigraphy of the Schneidermartin borehole (Fig. 2). The basin fill shows very variable reflection patterns that enable us to distinguish several seismic facies types. The high-resolution seismic acquisition allows us to follow reflections up to 10 m below the surface.

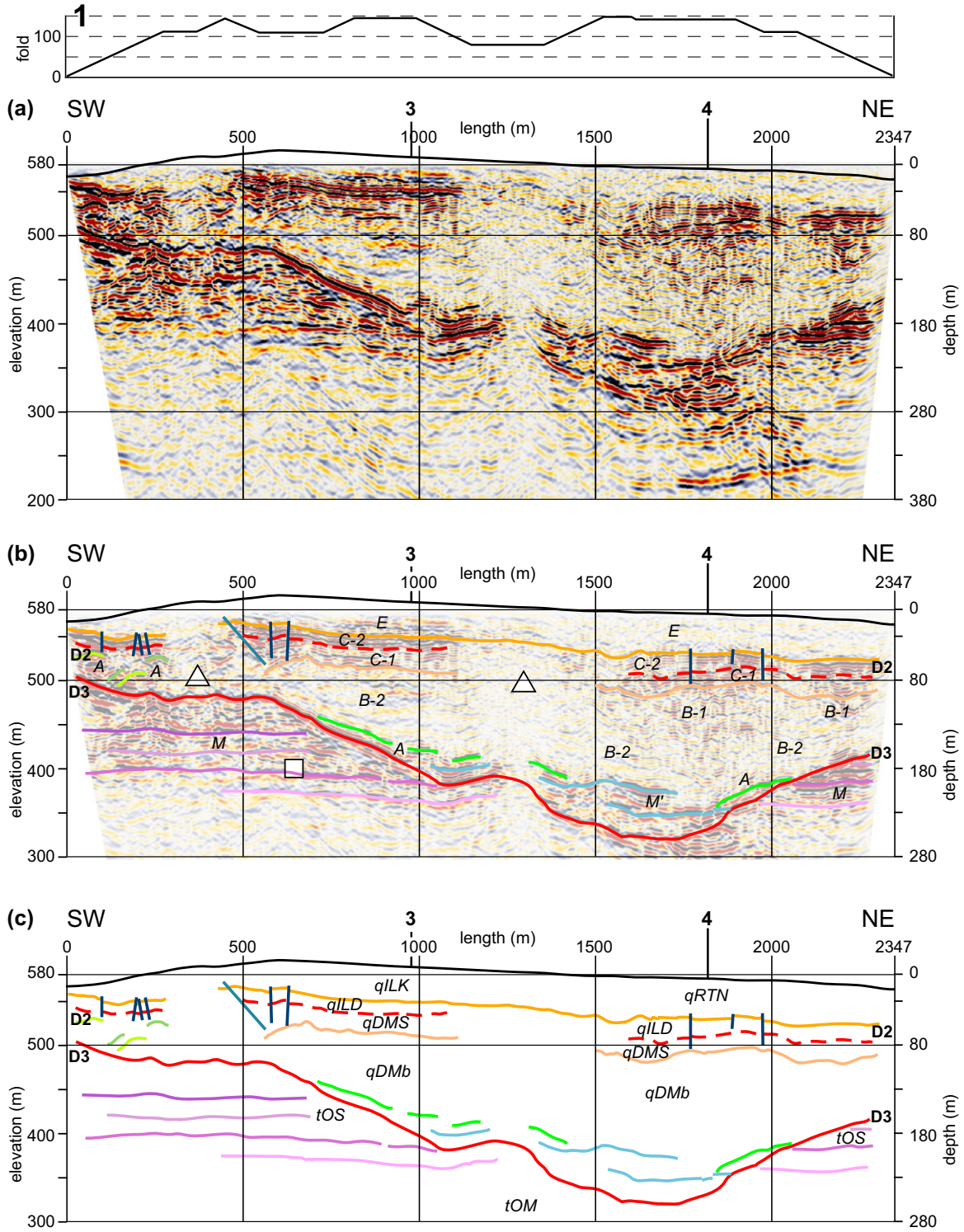

Figure 4 Profile 1. (a) Seismic section, (b) interpreted structure and seismic facies (cf. Table 4) superimposed on seismic section and (c) interpretation, including stratigraphic units (cf. Table 1). Vertical exaggeration, 2.5×. Profile intersections (black numbers), elevation (black line), seismic transparent regions (white triangle), foresets (white square), faults with offsets >2 m (dark blue), and faults with unknown offsets (light blue) are shown.

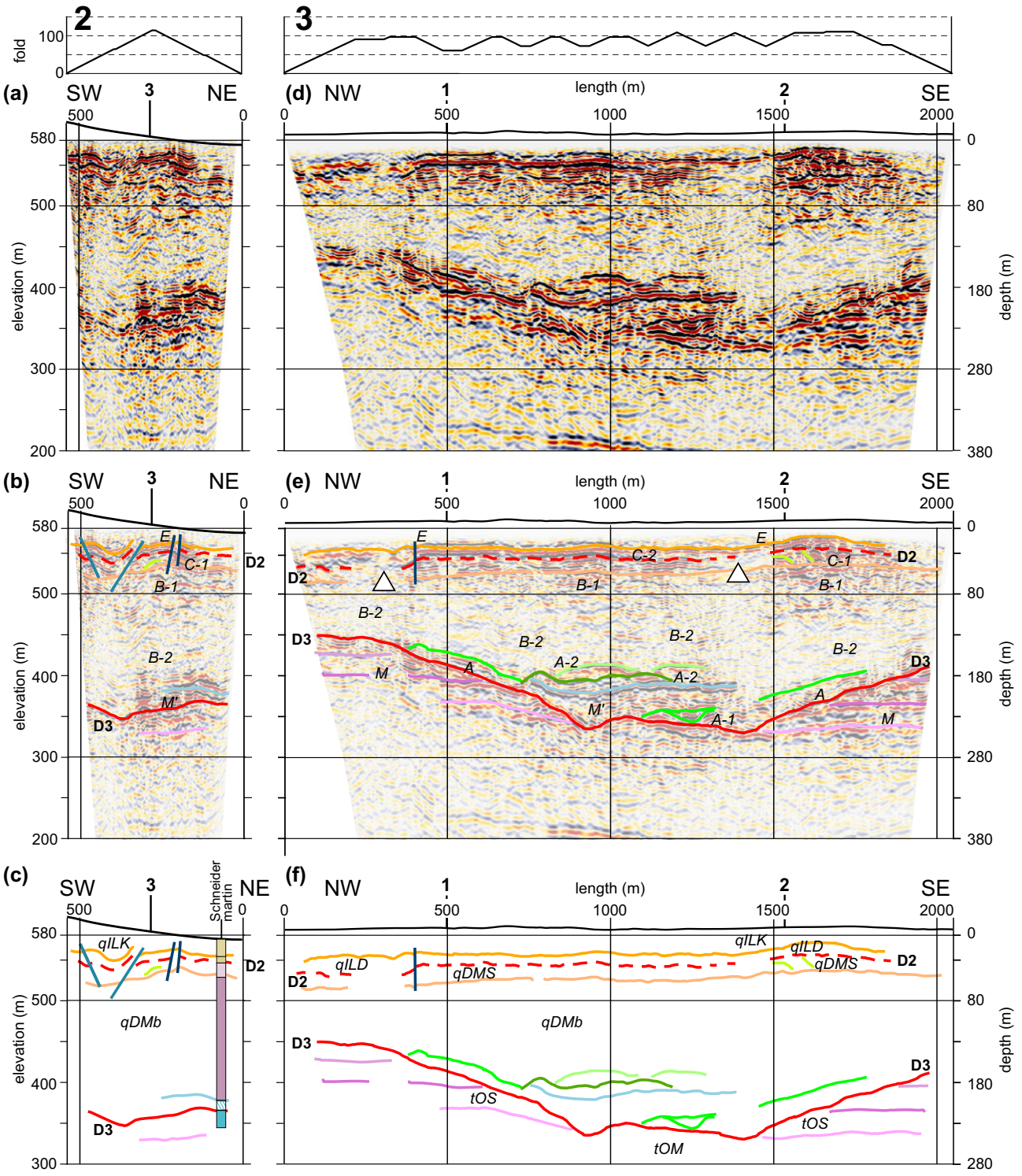

Figure 5 Profiles 2 and 3. (a, d) Seismic section, (b, e) interpreted structure and seismic facies (cf. Table 4) superimposed on seismic section and (c, f) interpretation, including stratigraphic units (cf. Table 1). For further explanation see Figure 4. Stratigraphy of the sediment succession of the Schneidermartin borehole (cf. Fig. 2) is superimposed on the geological interpretation of Profile 2 (c).

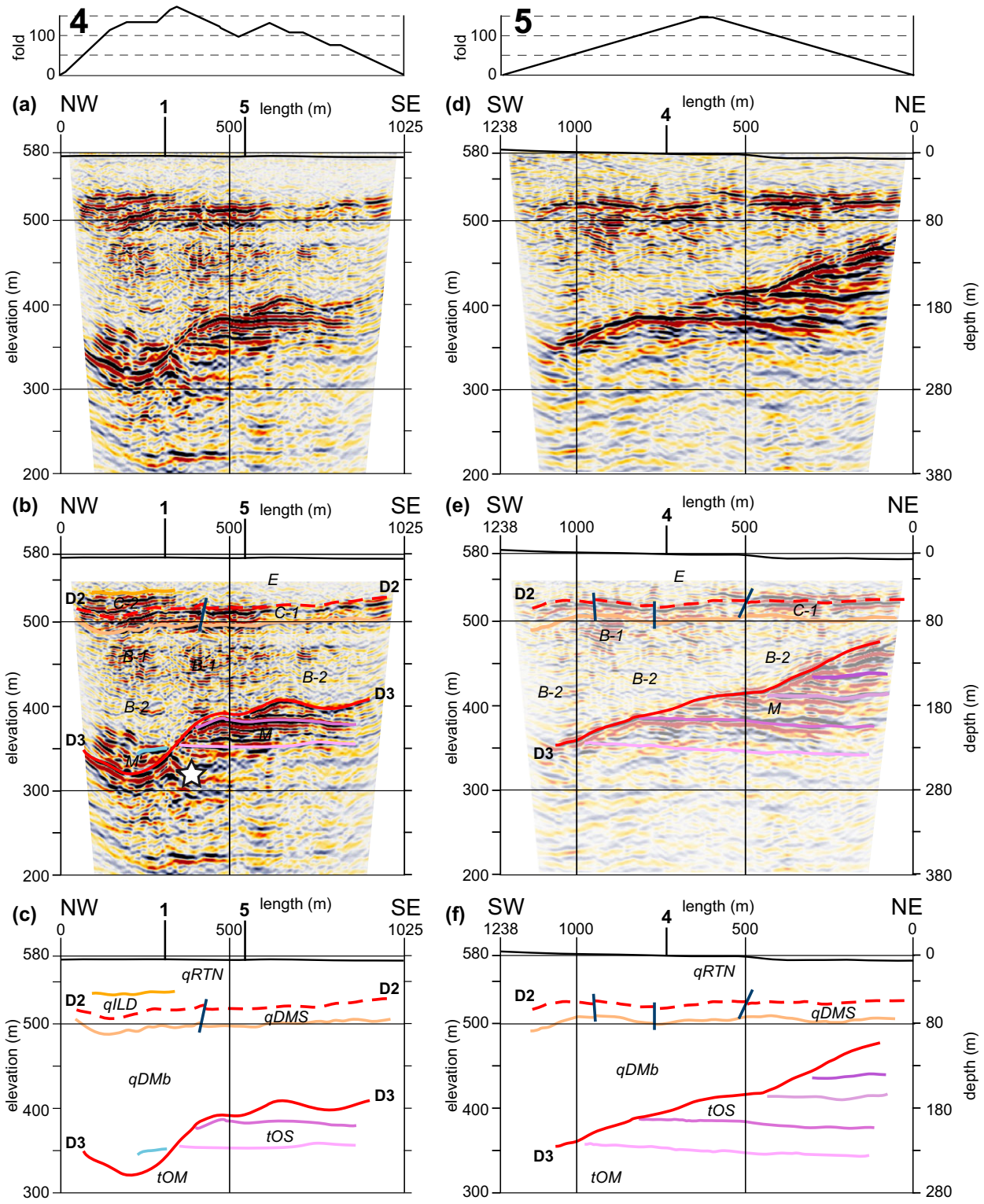

Figure 6 Profiles 4 and 5. (a, d) Seismic section, (b, e) interpreted structure and seismic facies (cf. Table 4) superimposed on seismic section and (c, f) interpretation, including stratigraphic units (cf. Table 1). A white star marks residuals of a strong diffraction on profile 4. Profile 5 was acquired using twice the shot- and geophone spacing with respect to other profiles. For further explanation, see Figure 4.

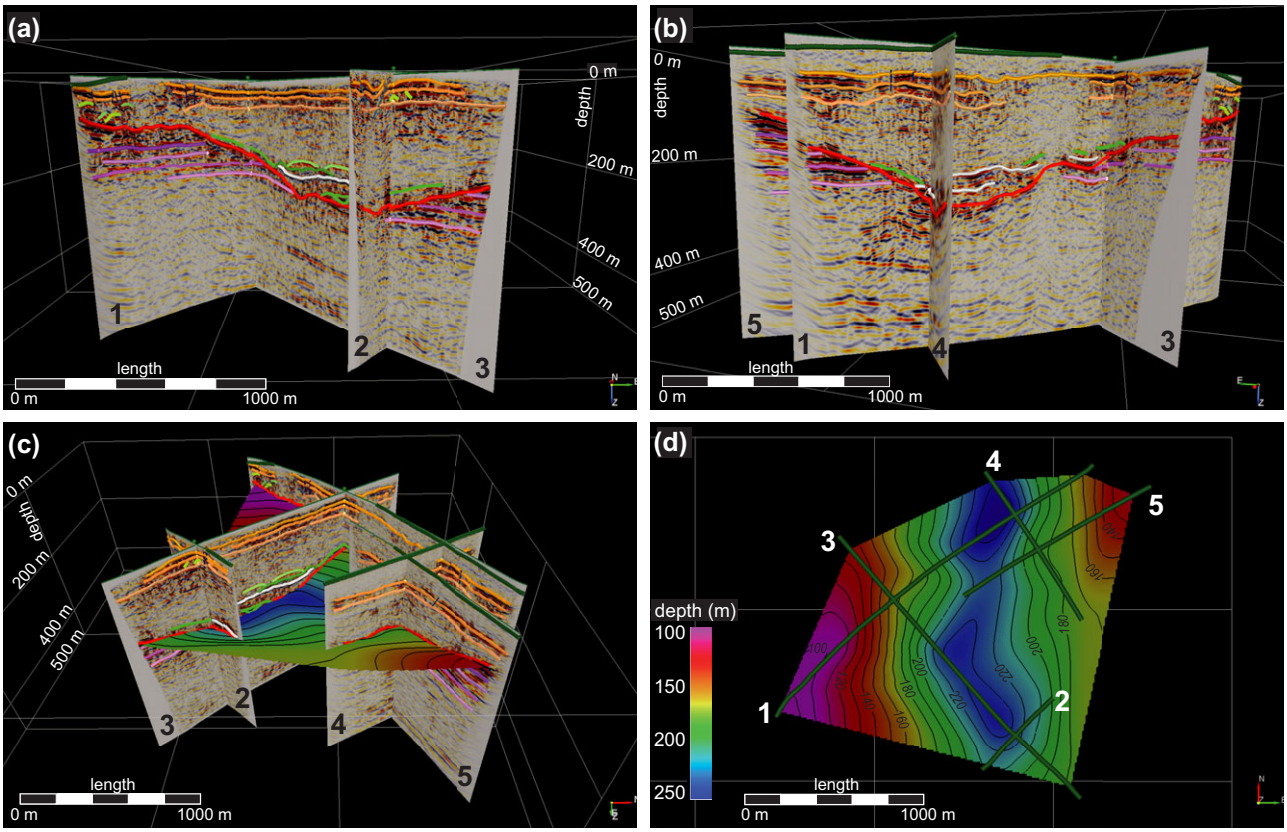

Figure 7 (a) Perspective three-dimensional view of the surveyed area, view towards the north, (b) view towards the south, (c) view towards the west with the triangulated, smoothed D3 unconformity surface and (d) depth map of the D3 unconformity surface. Scale for the front part of the model only. Note that the deepest part of the valley is elongated in a north–south direction.

Molasse units

The bedrock of the basin is composed of Tertiary molasse deposits that can be divided into two units: an upper, highly reflective part and a lower part with weak reflectivity. Four reflectors (M), at depths ranging from 80 to 245 m, can be traced on most sections inside the upper part (purple lines in Figs. 4–6). The molasse reflectors are clearly truncated by the basin on all profiles (except profile 2, which is too short), allowing a reliable interpretation of this unconformity. The upper part of the molasse units consists presumably of Upper Freshwater Molasse (*tOS*), which outcrops at the Venusberg (Fig. 1b). The lower part consists of Upper Marine Molasse (*tOM*), according to the sediment succession at the Schneidermartin borehole (Fig. 2).

The basin base – D3 unconformity

The erosional base of the Tannwald Basin, the D3 unconformity (cf. Table 1), is marked by a prominent reflector visible on all profiles (red lines in Figs. 4–6). The reflection signature of the D3 unconformity is a positive phase bounded by negative phases, clearly seen at the slope of profile 1 (Fig. 4, between lengths 500 and 1000 m). Since we recorded the data with normal SEG polarity, this implies an impedance increase. The D3 unconformity can be correlated uniquely in most parts of the basin, especially on the flanks, where the reflective layers of the molasse are truncated. In other parts, for example in the deeper part of profile 1 (Fig. 4), we were able to support our interpretation by using the cross profile 4.

The D3 unconformity incises through all the molasse reflectors and reaches a minimum elevation of ca. 320 m a.s.l. near the intersection of profiles 1 and 4, which means a maximum thickness of basin fill of 250 m. Profile 4 (Fig. 6a–c) very clearly shows a more than 50-m deep and several 100-m wide depression inside the basin, marking its deepest parts. This trough structure is similar to the deeper parts of the Bodensee Basin, that is, a Hasenweiler Basin (cf. Tab. 1), below Lake Constance (Wessels *et al.* 2015).

The flanks of the Tannwald Basin show prominent straight slopes, best visible on profiles 1 and 5 (Figs. 4 and 6d–f). Further to the west, the basin maintains a depth of about 80 m, as confirmed by the Wattenweiler borehole (Fig. 1b). If one extends the D3 unconformity with the same inclination toward the East, it fits well with the outcrop of Upper Freshwater Molasse (*tOS*) that forms the Venusberg (Fig. 1b).

Considering the interpretation of all profiles we identify the deepest part of the Tannwald Basin as a north–south elongated structure (Fig. 7) that varies from 150 to 250 m in depth. Two seismic refraction profiles (Behnke and Bram 1998), located north and south of our investigation area, show the D3 unconformity at a depth of ca. 170 m, so that we assume the basin continues to the north as well as to the south.

The basin infill

Based on reflection characteristics, we distinguish four different depositional sequences within the basin: the lowermost one is a highly reflective zone with distinct reflectors that occurs only in the deeper part of the basin. It is overlain by a thick sequence with low to medium reflectivity. This in turn is covered by a band of high and mostly continuous reflections. Above this, a nearly transparent region marks the top of the basin fill.

In the deepest part of the basin, strong reflectors occur above D3 unconformity, showing the same signature as below the D3 unconformity (blue lines in Figs. 4c, 5c and f and 6c). We interpret these as slabs of allochthonous molasse, internally undisturbed, that were relocated subglacially in the course of the basin erosion. This interpretation is confirmed by the core of the Schneidermartin borehole, where a 13-m thick allochthonous block of molasse shows evidence of glacial shearing (including thin layers of sheared fines directly on the undisturbed molasse bedrock, Fig. 2). At the base of this allochthonous block of molasse on profile 3 (length 750–1400 m; Fig. 5d–f), a channel structure of 50 m lateral and 10 m vertical dimensions is visible.

On top of the D3 unconformity as well as on top of the allochthonous molasse, we interpret a high-frequency reflector as the top of a layer of waterlain till (green lines in Figs. 4–6). On the basin flanks, this reflector is parallel to the D3 unconformity and indicates a constant thickness of this layer. On top of the allochthonous molasse slab, it is unclear whether the waterlain till was glacio-tectonically emplaced piggyback or deposited after the emplacement of the slab. It varies in thickness up to 15 m.

On profile 3, we identify two arch structures of ca. 20 m thickness and 250 m lateral extent (light green lines in Fig. 5d–f). They may represent a system of eskers that were deposited during the ice decay. Outside this central deep region, the flanks of the basin are overlain by D3 unconformity-parallel reflectors that we interpret as bordering subaqueous mass flows.

The reflective layers discussed so far are covered by a horizon that reaches a thickness of more than 100 m and displays relatively low reflectivity on all profiles. We interpret this unit as basinal fine-grained deposits of the Dietmanns basin sediments (*qDMb*). The reflectivity increases in the shallower parts, which can be explained by the occurrence of coarse-grained sediments in the upper part of this unit (Fig. 2). The depth of top *qDMb* increases slightly towards NE on profile 1 (Fig. 4) and NW on profile 4 (Fig. 6a–c).

Above the Dietmanns basin sediments (*qDMb*), a sequence of mainly horizontal oriented, parallel, strong reflectors occurs. We interpret (1) the basis of the Scholterhaus Sfm. (*qDMS*) as a continuous increase of reflectivity (orange line in Figs. 4–6). (2) The basis of Duermentingen Sfm. (*qILD*) occurs as a strong, continuous reflector accompanied by a series of less continuous horizontal reflectors below (red dashed line in Figs. 4–6). This reflector marks the D2 unconformity, which is developed locally as a concordant surface in the surveyed area. (3) The basis of the Kisslegg Sfm. (*qILK*), that is, the ice advance of the last glacial maximum (LGM), which correlates with the uppermost phase of a sequence of parallel reflections (dark orange line in Figs. 4–6). This reflector sequence is partially absent in the eastern part of the study area (Fig. 6), where glacial sediments were not deposited or subsequently eroded and replaced by melt-water deposits. On profile 2 (Fig. 5a-c), these units are interrupted by two opposingly dipping faults, which probably constitute a glacio-tectonic push structure at the outer margin of the LGM terminal moraine (*qILKe*). Push structures are also present in the westernmost portion of profile 1 (Fig. 4, length 0–300 m).

East of the terminal moraine (*qILKe*), we encounter sand and gravels of the outwash plain (*qRTN*) for the uppermost units. The diamictons of the glacial super-maximum (*qILK*), as indicated on the geological map (Fig. 1), are not covered by the seismic reflection profiles.

FACIES CHARACTERIZATION

In the previous section, we discussed the molasse units and the four major sedimentary units inside the basin. Each unit

shows different seismic signatures, which are not homogeneous within themselves (Table 4).

Facies M

Facies M shows mostly horizontal, often continuous reflectors with medium to high amplitude and medium frequency content. It can contain foresets (white square in Fig. 4b) as well. In the SW part of profile 1 (Fig. 4, length 250 m) and the NW part of profile 3 (Fig. 5d–f, length 300 m), the molasse reflectors are distorted, probably by static problems and/or a fluctuating velocity field. This facies represents Upper Freshwater Molasse units *(tOS)*. The lowermost units inside the Quaternary basin, interpreted as slabs of allochthonous molasse, show a similar reflection pattern, although they are more discontinuous, which may be due to their emplacement (facies M' in Figs. 4–6).

Facies A

Facies A describes medium to strong, continuous to discontinuous reflections with low frequency content. Reflection sequences can be traced in the range of 10s to 100s of metres. Reflector sequences are often parallel to each other, but sometimes onlap, for example on to the D3 unconformity. Layers may occur with variable thickness.

Facies A occurs on profiles 1 and 3, in the deepest parts of the basin, and constitutes the first basin refill after excavation. Therefore, we interpret these facies as waterlain till. On profile 3, high reflective and low frequency sub-facies A-1 show a trough structure as a channel at a depth of 220 m on profile 3. Sub-facies A-2 show medium reflectivity under an arch-shaped envelope and is the uppermost unit of facies A at a depth of 160 m, overlying the seismic facies M' (Table 4). We interpret these structures as eskers.

Facies B

Facies B varies between discontinuous to chaotic reflections with a low to medium reflectivity and high frequencies. Generally, the upper part of the seismic facies shows more horizontal and continuous reflectors (sub-facies B-1) with respect to the lower part (sub-faces B-2). The two sub-facies laterally grade one into each other. This facies can be observed on all profiles.

Facies B represents basinal fine-grained deposits of the Dietmanns basin sediments (*qDMb*). The higher amplitudes in the upper part of the seismic facies are presumably controlled by the coarsening-up sequence.

Facies C

Facies C is characterized by parallel reflectors with high reflectivity, frequency content, and amplitudes. The reflection pattern is mostly continuous, but is locally downthrown by faults that reach their higher density above the deepest part of the basin and show offsets of up to 3 m.

Facies C can be divided into a less continuous sub-facies C-1 and a more continuous sub-facies C-2. Sub-facies C-1 is characterized by reflection segments of lateral extent ranging from 10 to 100 m. The transition to facies B, located below, is gradual. Over a wide area, the top of sub-facies C-2 is marked by a prominent wavelet with a negative phase followed by a positive phase.

We interpreted facies C as superimposed till and sand units. The correlation with the lithostratigraphical data of the sediment succession at the Schneidermartin borehole allows us to identify sub-facies C-1 as Scholterhaus Sfm. (*qDMS*) and sub-facies C-2 as Duermentingen Sfm. (*qILD*). The high amplitudes of sub-facies C-2 were presumably controlled by the contrast of acoustic impedance due to the passage from coarse-grained gravels to fine-grained diamicton. In the centre of the basin, a higher fault density was probably caused by the greater compaction of the basin infill below. In the NE-part of profile 1 (Fig. 4), the onlap of *qILD* onto *qDMS* units can be clearly recognized.

Facies E

Facies E constitutes the uppermost unit (Table 4). Reflectivity is very low and chaotic so that it is almost transparent in the seismic reflection pattern. We interpret this as fluvially deposited sand and gravel of the outwash plain (*qRTN*) according to the surface geology (cf. geological map; Fig. 1).

GEOLOGICAL EVOLUTION

Based on the geological interpretation and facies characterization, we suggest the following evolution for the Tannwald Basin. During the Hosskirchian stage, glacial erosion incised a basin through the Upper Freshwater Molasse and, in the deepest parts, into the Upper Marine Molasse. The D3 unconformity forms the erosional base of this Dietmanns Basin.

Sedimentation began sub-glacially. Water-lain till was deposited forming a coarse-grained basal layer. Slabs of molasse

Table 4 Seismic Facies Characterization

Seismic Facies		Characteristics	Geometry	Geological Interpretation
M / M′	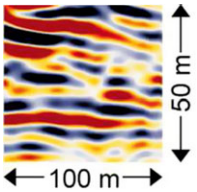	Medium to high amplitude, medium frequency content, marker horizons	Less continuous, less coherent, mostly horizontal and parallel, short reflection segments, may contain foresets	Upper Freshwater Molasse (*tOS)*, M' allochthonous molasse slab
A	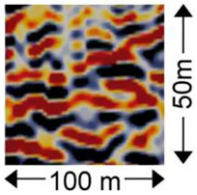	High amplitude, low-frequency content, abrupt termination of marker reflections	Continuous to discontinuous, partially parallel, lateral extent 10 to 100 seconds of metres, variable thickness	Lodgement till
A-1	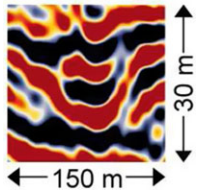		Trough structure, dimensions 100 m lateral, 20 m vertical	Channel
A-2	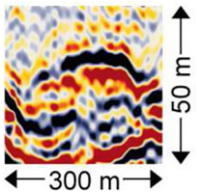		Arch structure, apparent dimensions up to 250 m lateral, 20 m vertical	Esker
B	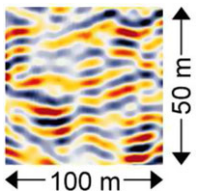	Low to medium amplitude, high-frequency content, gradual transition from low to medium amplitude	Discontinuous to chaotic, short to very short reflection segments with various dips, predominantly horizontal orientation	Basinal fine-grained deposits
B-1	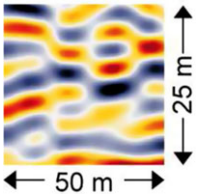	Medium amplitude	More horizontal, more continuous	Dietmanns basin sediment, *qDMb*
B-2	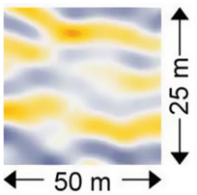	Low amplitude	Less horizontal, less continuous	

Continued

Table 4 Continued

Seismic Facies	Characteristics	Geometry	Geological Interpretation
C 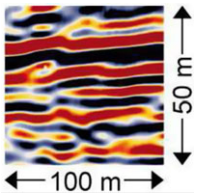	High amplitude, high frequency content	Mostly continuous, horizontal, parallel, sporadic interruptions, distinct boundaries	Till sequences and till, faults due to compaction
C-1 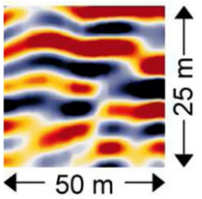		Less continuous and higher frequency content than A-1, parallel, coherent reflection segments	Scholterhaus Sfm., *qDMS*
C-2 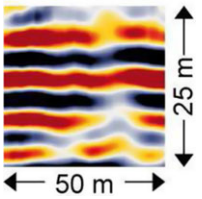	Wavelet with strong negative phase followed by strong positive phase	Very continuous, prominent reflection	Duermentingen Sfm., *qILD*
E 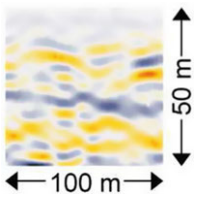	Very low amplitude, uppermost unit	Chaotic	Fluvial deposits, sand/gravel, outwash plains, *qRTN*

were ripped off the substrate, transported and deposited to different locations within the basin. The origin of such molasse slabs is until now unknown, but the depression on profile 4 (Fig. 6a–c) may represent a zone from which a molasse slab was plucked. The age of the channel that was incised into the molasse slab on profile 3 (Fig. 5d–f) is unclear. Other glacial landforms, such as the esker system on top of the molasse slab on profile 3 (Fig. 5d–f), were formed during ice decay. In the following ice-free environment, fine-grained lacustrine Dietmanns basin sediments (*qDMb*) were deposited as bottom sets and, later, as foresets (cf. fining-up and coarsening-up deposits at the Schneidermartin borehole; Fig. 2).

The next ice stage (Rissian stage) deposited till and sand of the Scholterhaus Sfm. (*qDMS*) and Duermentingen Sfm. (*qILD*). The ice advance did not erode a basin at this location, but instead outwash plain sediments were deposited. Thus, the D2 stratigraphical boundary at the base of the Duermentingen Sfm. is a conform surface in the Tannwald Basin.

The sedimentary record ended with last glacial maximum (LGM) terminal moraine (*qILKe*) in the first glaciation of the Wurmian stage, but sporadic minor ice advances further than the LGM locally deposited tills of the Kisslegg Sfm. (*qILK*). The lows of the peri-glacial landscape beyond the LGM were filled by glacio-fluvial gravels (*qRTN*), between the outcrops of the Kisslegg Sfm.

DISCUSSION

Data quality and previous studies

The dense acquisition proved to be necessary for an optimal imaging of the seismic facies units in the basin. Due to logistic

reasons, we measured profile 5 with double shot and receiver distances. For this reason, whereas the base of the basin and major boundaries inside could be well resolved, the facies of the basinal fine-grained deposits are not as well resolved as on the other profiles (Fig. 6d). This observation proves that a dense acquisition scheme is necessary for sufficient resolution.

At some locations a remarkable loss in signal strength of refractions as well as reflections could be observed (white hexagon in Fig. 3a). This results in large transparent areas in profiles 1 and 3 (white triangles in Figs. 4b and 5e). We explain this significant energy loss as due to a chaotic structure of laterally limited sedimentary units, where the wavefield is scattered and dampened. In the central part of profile 1, a high amount of near-surface diffractions in the un-migrated stack (not shown) indicates heterogeneously distributed scattering material in the deposits of the last glacial maximum (LGM), possibly blocks or boulders.

Below the basin flanks, reflectors often show pull-up due to the complex, strongly varying velocity field at these positions that could not be mapped precise enough in the tomography. This is also a reason for a diffraction residual on profile 4 (white star in Fig. 6b) that we could not completely migrate. The stacked section shows a very strong diffraction at this position. It is nearly impossible to achieve better velocity mapping, because this part of the basin is too deep and too complex to be resolved by refraction seismics, as can be seen from previous surveys (Behnke and Bram 1998). An improvement may come from full waveform inversion that might be able to capture the velocity field in more detail (e.g. Bleibinhaus and Hilberg 2012).

The depth of the basin determined by the seismic reflection survey coincides generally well with the results of the previous refraction seismics (Behnke and Bram 1998), where the boundary appears as a smoothed version of the unconformity found in our study. However, our results far exceed the refraction seismics in terms of the detail of the imaging of the structure and infill of the basin. For instance, at the deepest part of the basin, the refraction survey indicates a depth of only 200 m, whereas the maximum depth from our survey is 250 m. This probably results from the misinterpretation of compacted till layers and allochtonous slabs of molasse units as the D3 unconformity.

Comparison of this basin with other glacial basins

Büker *et al.* (1998, 2000) carried out the most detailed seismic investigation of an over-deepened alpine valley so far in the Swiss Suhre Valley. Their investigation area is located more proximally to the Alpine Glacier than our survey area and was covered by the last Wurmian ice advance, that is, it probably represents a later generation of basin erosion (equivalent to the D1 unconformity, Table 1). Nevertheless, some remarkable similarities in the seismic image exist; prominent quasi-continuous to short–high amplitudes reflections (interpreted as till layers), an up to 100-m thick nearly transparent zone, and strongly inclined reflections (highly compacted till or slabs of slumped basement, that is, molasse units). In the Tannwald Basin, we also envisage an allochtonous molasse block that was transported and deposited by the ice sheet, and placed on top of the D3 unconformity. The process of glacial plucking, as we hypothesize, is described by Bennett and Glasser (2011). This interpretation is based on seismic facies and is confirmed by the presence of sheared molasse blocks at the base of the Schneidermartin borehole. Compared to Büker *et al.* (1998, 2000), the molasse block in the Tannwald Basin exceeds dimensions of the slabs in the Suhre Valley and is separated from surrounding molasse. Morend *et al.* (2002) exposed facies of the Upper Freshwater Molasse from Lake Geneva with a similar appearance to our facies M. They showed a sediment succession that is similar to ours, but also stratigraphically one glacial cycle later with respect to the stratigraphy in the Tannwald Basin.

In Austria, geophysical investigations, including seismic reflection in the inner alpine basin of Hopfgarten (Tyrol), revealed the existence of three glacial sequences on top of each other, which are separated by single high-amplitude reflectors. These are interpreted as basal till and indicate the onset of a new glacier advance (Reitner *et al.* 2010). This is in accordance with our interpretation of the D2 unconformity as a major reflector. Brückl *et al.* (2010) distinguished an 'old valley fill' in the deepest parts of two Austrian valleys (Oichten and Drau Valleys) that show higher seismic velocities (2600 m/s) with respect to the upper part. Velocities exceeding 2500 m/s have been confirmed elsewhere in glacial valleys, for example Pugin *et al.* (2013) gave a value >2500 m/s for compacted till. The strong and rather continuous reflection pattern in the Oichten Valley displays a similar appearance to our facies unit 'A'. For this unit, we also found elevated velocities (~2300 m/s).

Quaternary glacial valleys are not confined only to the Alps, they are found worldwide. Some of them have been explored onshore using the seismic reflection method, for example in northern Germany (Wiederhold, Buness and Bram 1998), Denmark (Jørgensen and Sandersen 2009), Finland (Maries *et al.* 2016) and Canada (Pugin *et al.* 2009, 2014). Several of these studies investigated esker systems (Pugin *et al.*

2009, 2014; Maries *et al.* 2016). Maries *et al.* (2016) showed seismic facies of arched geometry and high amplitudes as well as dimensions of 100 m length and 20 m height, which is comparable to the eskers that we found in profile 3. The eskers described by Maries *et al.* (2016) appear to be more elongated (250 m) than in our sections, however this is probably because of the oblique cut, with regard to an assumed main ice flow direction toward the north. Pugin *et al.* (2009, 2014) exhibited several esker structures in Ontario and Saskatchewan, Canada. One of them, the buried Vars-Winchester Esker, shows a similar seismic signature to the eskers that we found.

CONCLUSIONS

The very dense acquisition schema, combined with a high-frequency vibroseismic source, proves to be well-suited to image this glacial over-deepened basin, from a maximum depth of ~250 m to only ~20 m below the surface. An essential prerequisite for a detailed and reliable interpretation is thorough processing of the data. In our case, a significant improvement, relative to DMO processing, is achieved by pre-stack depth migration (PSDM) processing. However, this comes at a cost, as PSDM needs several times more effort to iterate an appropriate velocity model. Furthermore, the transparent parts of the seismic section indicate that chaotic layering may impede seismic imaging almost totally.

The seismic reflection data allow us to distinguish various facies inside the basin fill. Strongly reflective glacial till can clearly be separated from less reflective basinal fine-grained deposits. A lithofacial interpretation is feasible on the basis of seismic data; however, reliable chrono-stratigraphical interpretation will be greatly improved by borehole information, since most of the Rhine Glacier area was affected by several glacial events (cf. Fig. 1). On the other hand, we suggest that other seismic investigations of glacial over-deepened valleys will be able to use our seismic facies characterization.

Besides the internal facies, we interpret structures such as small channels and eskers. The latter are of great significance hydrogeologically, since they constitute very permeable aquifers (Pugin *et al.* 2009; Maries *et al.* 2016) due to their coarse-grained composition. Due to their position at the base of the over-deepened valley they are presumably less affected by surface pollutants than shallower aquifers.

Based on the geological interpretation and the facies characterization, we hypothesize a geological evolution of the Tannwald Basin that is sustained by the sediment succession of the Schneidermartin borehole.

ACKNOWLEDGEMENTS

We thank our technical staff, Jan Bayerle, Eckhardt Grossmann and Sven Wedig, for their assistance in the field. We gratefully acknowledge funding by the German Research Foundation, grants GA74975-1 and KR2073/3-1. We thank the people of the village of Unteressendorf for their support. We thank the AE Ayse Kaslilar and the three anonymous reviewers for their thoughtful advice to improve the quality of this paper.

REFERENCES

Anderson R., Molnar P. and Kessler M. 2006. Features of glacial valley profiles simply explained. *Journal of Geophysical Research* **111**, F01004. https://doi.org/10.1029/2005JF000344.

Anselmetti F., Preusser F., Bavec M., Crouzet C., Fiebig M., Gabriel G. *et al.* 2016. Drilling overdeepened Alpine valleys (DOVE). ICDP Full Proposal, 174 pp.

Barnaba C., Marello L., Vuan A., Palmieri F., Romanelli M., Priolo E. *et al.* 2010. The buried shape of an alpine valley from gravity surveys, seismic and ambient noise analysis. *Geophysical Journal International* **180**, 715–733. https://doi.org/10.1111/j.1365-246X.2009.04428.x

Behnke C. and Bram K. 1998. Erforschung der würmzeitlichen Tannwald-Becken-Struktur (Fallgewichtseismik II – 1996). Report. *NlfB Archive* **116**:833.

Bennett M.M. and Glasser N.F. (Eds.). 2011. *Glacial Geology: Ice Sheets and Landforms*. John Wiley & Sons.

Bleibinhaus F. and Hilberg S. 2012. Shape and structure of the Salzach Valley, Austria, from seismic traveltime tomography and full waveform inversion. *Geophysical Journal International* **189**, 1701–1716.

Boenigk W. 1987. Petrographische Untersuchungen jungtertiärer und quartärer Sedimente am linken Oberrhein. *Jahresberichte und Mitteilungen des oberrheinischen geologischen Vereins NF* **82**, 113–129.

Bradford J., Liberty L., Lyle M., Clement W. and Hess S. 2006. Imaging complex structure in shallow seismic-reflection data using prestack depth migration. *Geophysics* **71**, B175–B181.

Brückl E., Brückl J., Chwatal W. and Ullrich C. 2010. Deep alpine valleys: examples of geophysical explorations in Austria. *Swiss Journal of Geoscience* **103**, 329–344. https://doi.org/10.1007/s00015-010-0045-x.

Buechi M.W., Frank S.M., Graf H.R., Menzies J. and Anselmetti F.S. 2017. Subglacial emplacement of tills and meltwater deposits at the base of overdeepened bedrock troughs. *Sedimentology* **64**, 658–685. https://doi.org/10.1111/sed.12319.

Büker F., Green A.G. and Horstmeyer H. 1998. Shallow seismic reflection study of a glaciated valley. *Geophysics* **63**, 1395–1407. https://doi.org/10.1190/1.1444441.

Büker F., Green A.G. and Horstmeyer H. 2000. 3-D high-resolution reflection seismic imaging of unconsolidated glacial and glaciolacustrine sediments: processing and interpretation. *Geophysics* **65**, 18–34. https://doi.org/10.1190/1.1444709.

de Franco R., Biella G., Caielli G., Berra F., Guglielmin M., Lozej A. *et al*. 2009. Overview of high resolution seismic prospecting in pre-Alpine and Alpine basins. *Quaternary International* **204**, 65–75. https://doi.org/10.1016/j.quaint.2009.02.011.

Dehnert A., Lowick S.E., Preusser F., Anselmetti F.S., Drescher-Schneider R., Graf H.-R. *et al*. 2012. Evolution of an overdeepened trough in the northern Alpine Foreland at Niederweningen, Switzerland. *Quaternary Science Reviews* **34**, 127–145. https://doi.org/10.1016/j.quascirev.2011.12.015.

Ehlers J. and Gibbard P.L. 2004. *Quaternary Glaciations – Extent and Chronology: Part I – Europe*, Vol. **2**. Elsevier.

Ellwanger D., Lämmermann-Barthel J. and Neeb I. 2003. Eine landschafts-übergreifende Lockergesteinsgliederung vom Alpenrand zum Oberrhein. *GeoArchaeoRhein* **4**, 81–124.

Ellwanger D., Wielandt-Schuster U., Franz M. and Simon T. 2011. The Quaternary of the southwest German Alpine Foreland (Bodensee-Oberschwaben, Baden-Württemberg, Southwest Germany). *Quaternary Science Journal* **60**, 306–328. https://doi.org/10.3285/eg.60.2-3.07.

Huuse M. and Lykke-Andersen H. 2000. Overdeepened Quaternary valleys in the eastern Danish North Sea: morphology and origin. *Quaternary Science Reviews* **19**, 1233–1253. https://doi.org/10.1016/S0277-3791(99)00103-1

Jørgensen F. and Sandersen P.B. 2009. Buried valley mapping in Denmark: evaluating mapping method constraints and the importance of data density. *Zeitschrift der Deutschen Gesellschaft für Geowissenschaften* **160**, 211–223.

LGRB. 2015. Lithostratigraphische Entwicklung des baden-württembergischen Rheingletschergebiets: Übertiefte Becken- und Moränen-Landschaft. LGRB Fachbericht 2015/4, Regierungspräsidium Freiburg, Freiburg i.Br, Germany. https://produkte.lgrb-bw.de/docPool/c525_data.pdf.

Litholex. 2017. Lithostratigraphisches Lexikon Deutschland 2016. http://litholex.bgr.de/.

MacGregor K.R., Anderson R.S., Anderson S.P. and Waddington E.D. 2000. Numerical simulations of glacial-valley longitudinal profile evolution. *Geology* **28**, 1031–1034.

Maries G., Ahokangas E., Mäkinen J., Pasanen A. and Malehmir A. 2016. Interlobate esker architecture and related hydrogeological features derived from a combination of high-resolution reflection seismics and refraction tomography, Virttaankangas, southwest Finland. *Hydrogeology Journal* **25**, 829–845. https://doi.org/10.1007/s10040-016-1513-9.

Morend D., Pugin A. and Gorin G.E. 2002. High-resolution seismic imaging of outcrop-scale channels and an incised-valley system within the fluvial-dominated Lower Freshwater Molasse (Aquitanian, western Swiss Molasse Basin). *Sedimentary Geology* **149**, 245–264. https://doi.org/10.1016/S0037-0738(01)00176-2.

Nitsche F.O., Green A.G., Horstmeyer H. and Büker F. 2002. Late quaternary depositional history of the Reuss delta, Switzerland: constraints from high-resolution seismic reflection and Georadar surveys. *Journal of Quaternary Science* **17**, 131–143. https://doi.org/10.1002/jqs.645.

Pfiffner O.A. 1986. Evolution of the north alpine foreland basin in the Central Alps. In: *Foreland Basins* (eds P.A. Allen and P. Homewood), pp. 219–228. Blackwell. https://doi.org/10.1002/9781444303810.ch11.

Pfiffner O.A. 2014. *Geology of the Alps*, 2nd edn. Wiley and Sons, New Jersey.

Pfiffner O.A., Lehner P., Heitzmann P., Mueller S. and Steck A. 1997. *Deep Structure of the Swiss Alps*. Springer.

Pomper J., Salcher B.C., Eichkitz C., Prasicek G., Lang A., Lindner M. *et al*. 2017. The glacially overdeepened through the Salzach Valley, Austria Bedrock: geometry and sedimentary fill of a major Alpine subglacial basin. *Geomorphology* **295**, 147–158.

Preusser F., Reitner J.M. and Schlüchter C. 2010. Distribution, geometry, age and origin of overdeepened valleys and basins in the Alps and their foreland. *Swiss Journal of Geosciences* **103**, 407–426. https://doi.org/10.1007/s00015-010-0044-y.

Pugin A.J.M., Brewer K., Cartwright T., Pullan S.E., Perret D., Crow H. *et al*. 2013. Near surface S-wave seismic reflection profiling – new approaches and insights. *First Break* **31**: 49–60.

Pugin A.J.M., Pullan S.E., Hunter J.A. and Oldenborger G.A. 2009. Hydrogeological prospecting using P-and S-wave landstreamer seismic reflection methods. *Near Surface Geophysics* **7**, 315–327. https://doi.org/10.3997/1873-0604.2009033.

Pugin A.J.M., Oldenborger G.A., Cummings D.I., Russell H.A. and Sharpe D.R. 2014. Architecture of buried valleys in glaciated Canadian Prairie regions based on high resolution geophysical data. *Quaternary Science Reviews* **86**: 13–23. https://doi.org/10.1016/j.quascirev.2013.12.007.

Reitner J.M., Gruber W., Römer A. and Morawetz R. 2010. Alpine overdeepenings and paleo-ice flow changes: an integrated geophysical-sedimentological case study from Tyrol (Austria). *Swiss Journal of Geosciences* **103**: 385–405. https://doi.org/10.1007/s00015-010-0046-9.

van Husen D. and Mayer M. 2007. The hole of Bad Aussee; an unexpected overdeepened area in NW Steiermark, Austria. *Austrian Journal of Earth Sciences* **100**, 128–136.

van Rensbergen P., de Batist M., Beck C. and Chapron E. 1999. High-resolution seismic stratigraphy of glacial to interglacial fill of a deep glacigenic lake: lake Le Bourget, Northwestern Alps, France. *Sedimentary Geology* **128**, 99–129. https://doi.org/10.1016/S0037-0738(99)00064-0.

van Rensbergen P., de Batist M., Beck C. and Manalt F. 1998. High-resolution seismic stratigraphy of late Quaternary fill of Lake Annecy (northwestern Alps): evolution from glacial to interglacial sedimentary processes. *Sedimentary Geology* **117**, 71–96. https://doi.org/10.1016/S0037-0738(97)00123-1.

von Hartmann H., Tanner D.C. and Schumacher S. 2016. Initiation and development of normal faults within the German Alpine Foreland Basin: the inconspicuous role of basement structures. *Tectonics* **35**, 1560–1574. https://doi.org/10.1002/2016TC004176.

Wessels M., Anselmetti F., Artuso R., Baran R., Daut G., Gaide S. *et al*. 2015. Bathymetry of Lake Constance – a high-resolution survey in a large, deep lake: *Zeitschrift für Geodäsie. Geoinformation und Landmanagement* **4**, 203–210. https://doi.org/10.12902/zfv-0079-2015.

Wiederhold H., Buness H. and Bram K. 1998. Glacial structures in northern Germany revealed by a high-resolution shallow reflection survey. *Geophysics* **63**, 1265–1272.

Ziegler P.A., Cloetingh S. and van Wees J.D. 1995. Dynamics of intraplate compressional deformation: the Alpine foreland and other examples. *Tectonophysics* **252**, 7–59, https://doi.org/10.1016/0040-1951(95)00102-6.

